Semi-Annual Status Report

to the

National Aeronautics and Space Administration

on

Grant NGL 44-012-006

"Millimeter Wavelength Spectroscopy and Continuum Studies of the Planets"

for the period

1978 October 1 to 1979 March 31

Co-Principal Investigators

Paul A. Vanden Bout
Assoc. Prof. Astronomy
(512) 471-4477

John H. Davis
Asst. Prof. Electrical Engineering
(512) 471-4651

Electrical Engineering Research Laboratory
The University of Texas at Austin
Balcones Research Center
10100 Burnet Road
Austin, TX 78758

The NASA Technical Officer for this grant is Dr. William E. Brunk, NASA Headquarters, Planetary Programs, Office of Space Science, Code SL, 400 Maryland Ave., S.W., Washington, D. C. 20546.

INTRODUCTION

The effort during this period has concentrated on reduction of data already in hand. This includes data mainly for two projects: the absolute brightness temperature measurements at 86.1 GHz and the spectral line observations of Venus.

The latter, mainly CO observations at 115 GHz, have been assembled into a common data base and are being searched for variation patterns. We plan to write up the results for submission this fall to a journal. The results of the former experiment have been written up and submitted to IEEE - Transactions on Antennas and Propagation. A copy of the manuscript is attached.

Absolute Brightness Temperature Measurements at 3.5 MM Wavelength

B. L. Ulich, Member, IEEE, J. H. Davis, Member, IEEE,
P. J. Rhodes, and J. M. Hollis

B. L. Ulich, P. J. Rhodes, and J. M. Hollis are with the National Radio Astronomy Observatory (NRAO), Tucson, AZ 85705. The NRAO is operated by Associated Universities, Inc., under contract with the National Science Foundation.

J. H. Davis is with the Millimeter Wave Observatory (MWO), Department of Electrical Engineering, The University of Texas at Austin, TX 78712. The MWO is operated by the Electrical Engineering Research Laboratory, The University of Texas at Austin, with support from the National Aeronautics and Space Administration, the National Science Foundation, and McDonald Observatory.

Abstract - Careful observations have been made at 86.1 GHz to derive the absolute brightness temperatures of the Sun (7914 ± 192 K), Venus (357.5 ± 13.1 K), Jupiter (179.4 ± 4.7 K), and Saturn (153.4 ± 4.8 K) with a standard error of about 3 %. This is a significant improvement in accuracy over previous results. A stable transmitter and novel superheterodyne receiver were constructed and used to determine the effective collecting area of the MWO 4.9 m antenna relative to a previously calibrated standard gain horn. The thermal scale was set by calibrating the radiometer with carefully constructed and tested hot and cold loads. The brightness temperatures may be used to establish an absolute calibration scale and to determine the antenna aperture and beam efficiencies of other radio telescopes at 3.5 mm wavelength.

I. INTRODUCTION

The absolute intensity of a celestial radio source is difficult to measure accurately at millimeter wavelengths, primarily because of instrumental difficulties, but it conveys more information useful to theorists than any other observable parameter of electromagnetic radiation. The short wavelengths employed require extreme precision in the fabrication of microwave hardware. The relatively high losses of typical waveguide components and the poor performance of detectors combine to significantly increase the noise temperature of millimeter wavelength radiometers over their lower frequency counterparts. In addition, the precise surfaces required for filled-aperture antennas at short wavelengths severely limit the effective collecting area of existing radio telescopes. The Earth's atmosphere will also significantly attenuate celestial radio signals due to absorption by molecular oxygen and water vapor [1]. The net result of these difficulties is a relatively imprecise absolute calibration scale for millimeter-wavelength radio astronomical observations. The purpose of this experiment is to improve the accuracy of the absolute flux density scale at 3.5 mm wavelength by employing new techniques for antenna gain calibration, thermal noise calibration, and impedance mismatch corrections, and by the construction of a stable transmitter and receiver specifically designed to reduce the dominant measurement errors.

II. INSTRUMENTATION

The system used to detect celestial radio emission consists of a conventional paraboloidal reflector antenna with a superheterodyne Dicke radiometer located at the prime focus. The thermal emission from blackbody loads is used to calibrate the absolute intensity of the detected signals. The effective collecting area of the paraboloid is determined by comparing the signal received from a continuous wave (CW) transmitter located some distance from the receiving equipment with the signal from a previously-calibrated standard gain horn. The same general procedure has been previously used to provide absolute flux density calibrations of radio sources at 2.3 GHz {2}, 20.5-35.5 GHz {3}, 35.0 GHz {4}, 97.1 GHz {4}, and 141 GHz {5}.

A. Paraboloidal reflector

The antenna is the 4.88 m diameter, f/0.5 paraboloidal reflector {6}, {7} operated by the Millimeter Wave Observatory on Mt. Locke, Texas at an altitude of 2015 m. In order to minimize atmospheric propagation loss, a high-altitude telescope site was chosen in an arid, cloud-free climatological zone. The RMS random telescope tracking error is 2 arc seconds, and the corrections to measured intensities due to tracking jitter are negligibly small ($\simeq$ 0.04 %). The systematic pointing error is 13 arc seconds RMS, and significant intensity errors can result if this pointing error is not corrected or taken into account properly. For these observations a five point grid centered on the nominal source position was mapped in order to measure the systematic pointing residuals and to correct the measured intensities. The reflector profile has an RMS deviation from a paraboloid of only about

0.1 mm, insuring good aperture efficiency and nearly diffraction-limited performance throughout the millimeter band. The radiation patterns measured at 86.1 GHz (wavelength λ = 3.482 mm) on the pattern range are shown in Fig. 1.

B. Calibration horn

The calibration horn used as a gain standard has been previously described by Ulich {8}. It is a simple conical horn with an axial length of 121.92 cm and an aperture of 10.16 cm. At 86.1 GHz the far-field directivity was determined to be 37.202 ± 0.030 dB (all errors quoted in this paper are one standard deviation) using a radiometric calibration scheme similar to the "artificial moon" technique {9}. This conical horn was also used to measure the average disk brightness temperature of the Sun and to perform sky "tipping" scans to monitor atmospheric extinction. Measured radiation patterns at 86.1 GHz are shown in Fig. 2. Fig. 3 is a plot of the spillover efficiency (i.e., the normalized fraction of radiated power which is contained within a cone of specified half-angle) calculated from the measured patterns. At 86.1 GHz the measured horn dissipation loss is only 2.0 ± 0.5 %, which agrees with the calculated value of 2.3 % {8}.

C. Transmitter

A CW transmitter was constructed to provide a strong signal for the relative directivity measurements of the paraboloid and the calibration horn. A phase-locked klystron at 86.100 GHz provided power to a lens-corrected conical horn antenna with about 33 dB gain. As shown in the block diagram of Fig. 4, a feedback control circuit was used to maintain constant transmitted power. Laboratory measurements

indicate a typical stability of about 0.04 dB/hour. The entire transmitter is contained in a thermally insulated box to reduce errors caused by temperature fluctuations. The transmitting horn was carefully aligned to the direction of the telescope to insure uniform illumination of the paraboloid.

D. Receiver

A multipurpose receiver was also constructed to enable three types of observations to be conveniently made. Fig. 5 is a block diagram showing the significant subsections of the receiver. The first mode of operation is that of a single-conversion, phase-locked, narrowband superheterodyne receiver with an intermediate frequency (IF) of 30 MHz. An accurate waveguide below cutoff (WBCO) attenuator (Airborne Instruments Laboratory Type 3232) is used with the IF substitution technique [10] to determine the ratio of the transmitter power received by the paraboloid to that received by the standard gain horn. The accuracy of the WBCO attenuator calibration is ±{0.03 dB + (0.005 dB per 10 dB change in reading)}. The waveguide switch at the receiver input allows rapid comparison of the signals from the paraboloid feed horn and from the calibration horn which is physically coaxial with the telescope axis. The WBCO attenuator is preceded by a high-power, heat-sunk transistor amplifier (+29 dBm for -1 dB compression) to insure adequate dynamic range to accommodate the 33 dB difference in received signal level without significant IF saturation. A 30 MHz bandpass filter reduces the bandwidth of the detected spectrum and improves the signal-to-noise ratio. In operation, a change in radio frequency (RF) signal level is compensated by WBCO attenuation of the IF signal to maintain a constant detector output. All waveguide flanges and other sites of possible RF leakage are wrapped with copper

foil tape to insure sufficient isolation between the paraboloid and the calibration horn. Special observations were made in an effort to detect residual leakage, but none was found at a level -23 dB below the calibration horn signal.

The second mode of receiver operation is that of a broadband Dicke superheterodyne radiometer. In this mode the IF bandpass is from 10 to 500 MHz. The receiver noise temperature was measured to be 6100 K (double sideband) at the input, and the ΔT_{RMS} was 0.6 ± 0.1 K for one second of integration time, which agrees with the theoretical value of 0.55 K. A switchable circulator alternately connects the receiver to one of two identical feed horns at a 20 Hz rate. The feeds are optimized pyramidal horns which have aperture dimensions of 0.90 λ in the E-plane and 1.25 λ in the H-plane. The feed spacing resulted in an orthogonally polarized reference beam separation of 2.6 half-power beamwdiths off-axis in hour angle. Observations of blackbody calibration loads and of celestial radio sources were made using the broadband radiometer output.

The third mode of receiver operation is that of a reflectometer. An integral waveguide slotted line was used to measure the reflection coefficients of the various antennas, of the thermal calibration loads, and of the receiver input.

E. Thermal calibration loads

Absolute noise power spectral density calibration was obtained by observing the difference in signal level from two loads. Both loads were fabricated using Eccosorb CV-3 porous carbon-impregnated

foam absorber (Emerson and Cuming, Inc., Canton, MA) enclosed in an aluminum cavity {11}. One load was nominally at ambient temperature, and a laboratory thermometer inserted in the absorber was used to determine its physical temperature. The second load was insulated on all sides with 5.1 cm of expanded polystyrene and filled with liquid nitrogen. The foam walls (density = 0.032 g cm^{-3}) have an estimated relative dielectric constant of 1.029 and a loss tangent of about 3.6×10^{-5} near 3 mm wavelength based on measurements of polystyrene at 90 GHz {12} and density scaling laws {13}. The calculated power reflection of the foam wall is 0.02 % and the absorption is 0.33%. The measured transmissivity was 0.9969 ± 0.0007 at 86.1 GHz, which agrees within the error with the calculated value of 0.9965.

III. VSWR MEASUREMENTS

The waveguide slotted line built into the receiver was used to measure the voltage standing wave ratio (VSWR) of system components, and the results are given in Table I. The magnitudes of the voltage reflection coefficients ($|\Gamma|$) at 86.1 GHz are generally quite low. The receiver input is the worst match of the components tested even though an isolator (see Fig. 5) has been used to improve the impedance matching. Measurements of the mixer without the isolator indicated an input VSWR of 2.7, so it appears that the isolator does significantly improve the matching. The reflection coefficient of the 4.9 m paraboloid was determined by axially focusing the receiver box. Theoretical calculations {14} predict a value of 0.0012, which agrees with the measurement. The

TABLE I

86.1 GHZ VSWR DATA

Source	$\|\Gamma\|$	VSWR
Calibration horn	0.029 ± 0.001	1.060 ± 0.002
Reflector feed horn	0.024 ± 0.001	1.049 ± 0.002
4.9 M Paraboloidal reflector	0.0015 ± 0.0005	1.003 ± 0.001
Ambient temperature load	0.0020 ± 0.0005	1.004 ± 0.001
Eccosorb CV-3 absorber	0.0020 ± 0.0005	1.004 ± 0.001
Liquid nitrogen cooled load	0.044 ± 0.002	1.092 ± 0.004
Receiver waveguide switch input	0.076 ± 0.003	1.165 ± 0.006

thermal calibration loads and the absorber were measured using a traveling mechanical stage in front of the calibration horn. These data were taken at normal incidence and corrections due to waveguide loss were determined by observations of a copper shorting plate. Measurements of the liquid nitrogen cooled load with cryogen ($|\Gamma| = 0.044 \pm 0.002$) and without cryogen ($|\Gamma| = 0.011 \pm 0.002$) indicate that the dominant source of reflection is the foam-cryogen interface.

All pattern range, thermal calibration, and radio source measurements have been corrected for mismatch loss {15}. However, since only the amplitudes of the reflection coefficients (and not the phases) are known, an "exact" correction cannot be made in general. We have chosen to set the conjugate mismatch loss factor equal to the mean of its maximum and its minimum possible values and, for the purpose of conservative error analysis, to estimate an error of one standard deviation by the maximum possible error. Thus the mean mismatch loss correction factor between components 1 and 2 is (assuming small reflection coefficients)

$$\langle M \rangle \equiv \frac{\text{Power dissipated in load}}{\text{Maximum available power}} = (1-|\Gamma_1|^2)\ (1-|\Gamma_2|^2) \qquad (1)$$

and the estimated 1σ error is

$$\Delta M \equiv 2|\Gamma_1|\ |\Gamma_2|. \qquad (2)$$

The effect of mismatch on the broadband radiometric data (instantaneous bandwidth ~ 1 GHz) is less serious than for the coherent measurements since the detector will in most cases average the signal over several cycles of the sinusoidal standing wave pattern, and the mismatch factor given by (1) will then be nearly correct. In this case the true mismatch error will be overestimated by (2).

IV. PATTERN RANGE MEASUREMENTS

An unobstructed pattern range was used to provide a quasi-plane wave input to the 4.9 m paraboloid and to the coaxial calibration horn for the narrowband directivity comparison measurements. The transmitter site was a hilltop in the Davis Mountains State Park at an altitude of 1680 m and a range of 12.9 km from the MWO. As seen from the telescope, the transmitter is at -1.5° elevation angle, and the closest possible ground reflection is about 0.63° below that angle (i.e., about 13 beamwidths off-axis). A search for signals near this angle indicated that ground reflections were negligibly small (less than -30 dB with respect to the direct path). The finite range of the transmitter, however, means that the wave impinging on the telescope is not planar, but rather spherical, and the resulting quadratic phase error produces some reduction in peak gain of the paraboloid. Fortunately, a degree of freedom exists in the telescope which can be utilized to simulate far-zone radiation patterns in the Fresnel zone. At a range R = 12.9 km the transmitter is $1.89\ D^2/\lambda$ from the paraboloid (of diameter D). By defocusing the feed horn axially away from the reflector (of focal length f) by a distance ε, the far-zone radiation pattern can be

virtually duplicated for ranges greater than $0.5D^2/\lambda$. The axial defocusing distance ε is given by

$$\varepsilon = \frac{Kf^2}{R}\left\{1 + \left[\frac{1}{4(f/D)}\right]\right\}^2 \qquad (3)$$

where $K = 0.92$ {16} . The peak gain of the antenna is the same whether it is focused in the Fresnel zone or at infinity {17} . First the feeds were focused to receive maximum transmitter signal and the directivity comparison data were taken. Then the feeds were axially displaced by 0.15 λ (calculated from (3)) toward the reflector to focus at infinity, and the planetary radio observations were made at this setting. In this case the expected gain reduction if the feeds were not refocused is only about 1.4 %.

Figure 6 is a plot of the variation in signal power received by the paraboloid during a typical 20 minute period. Most of the noise is due to atmospheric scintillation, and data were taken between midnight and sunrise to minimize errors due to fading. Table II presents individual measurements of the observed signal power ratio. Some of these measurements were made at lower transmitter power levels to search for possible receiver nonlinearity due to saturation, but in no case was any nonlinearity detected. A calibrated rotary-vane RF attenuator in the transmitter was also used to check the WBCO IF attenuator calibration, and no nonlinearity was detected within the accuracy of the RF attenuator calibration (± 0.1 dB). Each measurement was made after careful pointing adjustments to maximize the received signals.

TABLE II

ANTENNA SIGNAL RATIO DATA

Trial	Date	UTC (Hours)	Signal from reflector / Signal from horn (dB)
1	12/14/77	0500	32.914
2	12/14/77	0900	32.885
3	12/15/77	0400	32.924
4	12/15/77	0900	32.928
5	12/15/77	1400	32.930
<1-5>	-	-	32.916 ± 0.008

The reflector directivity (referred to the aperture plane of the on-axis feed) is simply obtained by correcting the observed signal power ratio for the different losses of the paths from the feed horn and the calibration horn to the ferrite switch and then multiplying by the directivity of the calibration horn. As indicated in Table III, the directivity of the 4.9 m reflector at 86.1 GHz is 70.160 ± 0.072 dB. The estimated uncertainty is the quadrature sum (root sum of squares) of the estimated errors (which are assumed to be independent) in the calibration horn directivity, signal power ratio repeatability, mismatch correction, receiver gain correction repeatability, WBCO attenuator calibration, polarization angle misalignment, refocusing, and difference in cross polarization. This last uncertainty exists because the calibration horn directivity was determined using an unpolarized source, whereas for the directivity ratio experiment a linearly polarized source was used. Table IV summarizes the measured parameters of the calibration horn and of the paraboloid. The reflector has a high aperture efficiency (53.58 ± 0.89 %), indicating that surface errors are much smaller than a wavelength and that the radiation pattern is nearly diffraction-limited. The reflector half power beamwidths are also essentially equal since the aperture dimensions of the pyramidal feed horn have been chosen to produce a main lobe with a circular cross section.

V. THERMAL CALIBRATION

The noise power P (W) delivered to the receiver in a single polarization through the aperture of either the on-axis feed horn or the calibration

TABLE III

REFLECTOR DIRECTIVITY

Quantity	Value (dB)
Calibration horn directivity	37.202 ± 0.030
Ratio of reflector signal to horn signal	32.916 ± 0.008
Uncertainty due to mismatch	± 0.026
Ratio of receiver gain at calibration horn aperture to gain at reflector feed aperture	0.04 ± 0.018
Uncertainty in WBCO attenuation	± 0.046
Uncertainty due to polarization angle misalignment	± 0.005
Uncertainty in refocusing	± 0.025
Uncertainty due to difference in cross polarization	± 0.022
Reflector directivity at horizon	70.160 ± 0.072

TABLE IV

ANTENNA PARAMETERS AT 86.1 GHZ

Quantity	Calibration Horn	Paraboloidal Reflector
Diameter (m)	0.1016	4.877
Geometrical area (m^2)	0.008107	18.679
Directivity (dB)	37.202 ± 0.030	70.160 ± 0.072
Effective area (m^2)	0.005065 ± 0.000036	10.010 ± 0.166
Aperture efficiency (%)	62.48 ± 0.44	53.58 ± 0.89
HPBW in E-plane (arc minute)	127 ± 2	2.91 ± 0.03
HPBW in H-plane (arc minute)	152 ± 2	2.86 ± 0.03

horn from a perfectly matched (blackbody) load at an absolute physical temperature T enclosed in a perfectly conducting cavity is given by

$$P = k\,B\,J(T) \tag{4}$$

where k is Boltzmann's constant (1.38054×10^{-23} J K^{-1}), B is the predetection bandwidth (Hz), and the effective radiation temperature J(T) is given by

$$J(T) = \frac{(h\nu/k)}{\exp(h\nu/kT) - 1} \tag{5}$$

In (5) h is Planck's constant (6.6256×10^{-34} J s) and ν is the frequency (Hz). In practice the bandwidth B is usually not precisely known, and microwave radiometers are generally calibrated in terms of the effective radiation temperature J(T), which is proportional to noise power spectral density. When $h\nu \ll kT$, $J(T) \approx T$, and the familiar concept of antenna temperature may be used in the Rayleigh-Jeans approximation to the Planck distribution.

The broadband radiometric observations of the Sun and planets were calibrated by first comparing the signal from a neon noise tube to that from the hot and cold loads. The calibrated noise tube signal was then used as a secondary transfer standard to allow rapid and convenient calibration of celestial radio sources. In practice the noise tube was constantly on to avoid thermal output drift, and a ferrite modulator was turned on and off under computer control to generate the calibration signal. Table V presents a summary of the noise tube calibration measurements, which were interleaved in time with the radio source observations to reduce systematic errors. Alternate observations of the hot and cold loads over the apertures of the on-axis feed horn and of the calibration

horn were also used to determine the relative receiver gain from these two input ports to the square law detector. As indicated in Table V, simultaneous recordings of ambient (hot load) temperature T_{AMB} and of barometric pressure were used to determine the radiation temperature difference of the two loads. The boiling point of liquid nitrogen T_{LN} (K) is related to the barometric pressure P_B (mm Hg) by [18]

$$T_{LN} = 77.36 + 0.011\ (P_B - 760) \tag{6}$$

and the microwave absorber is physically at this temperature since it is completely immersed in the cryogen. The foam wall, however, attenuates the emission from the absorber and also emits radiation according to its normalized power loss factor α. For small losses the effective radiation temperature $J(T_C)$ of the cold load is

$$J(T_C) = J(T_{LN}) + (\alpha/2)\left[J(T_{AMB}) - J(T_{LN})\right] \tag{7}$$

where a linear temperature gradient in the foam wall has been assumed and reflections are neglected [18]. In the present case $\alpha = 0.0033$ and the foam wall increases the effective cold load temperature by about 0.3 K. This was experimentally verified by comparison measurements of a second cold load without the foam wall. A 45^{o} flat reflector was placed above an absorber-lined cavity filled with cryogen, and the signal was found to be within $\pm$ 0.4 K of the cold load with foam. Measurements made with a second foam wall in place indicated an increase of 0.9 $\pm$ 0.4 K, which agrees with the calculated value of 0.7 K. Thus the low loss of the foam wall and its small effect on the cold load temperature has been confirmed.

TABLE V

THERMAL CALIBRATION DATA

Trial	Date	UTC (Hours)	Barometric Pressure (MM Hg)	Receiver Total Power Output (Volt)	T_{AMB} (K)	T_{LN} (K)	$T_{AMB} - T_{LN}$ (K)	$\frac{\Delta CAL}{\Delta H/C\ (Feed)}$	$\frac{\Delta H/C\ (Feed)}{\Delta H/C\ (Horn)}$	T_{CAL} (K)
1	12/15/77	0000	609	0.923	281.3	75.7	205.6	0.1389	1.0055	28.30
2	12/16/77	0200	603	0.917	284.4	75.6	208.8	0.1428	0.9945	29.53
3	12/17/77	0300	605	0.920	280.1	75.7	204.4	0.1459	0.9933	29.54
4	12/18/77	0300	609	0.938	280.5	75.7	204.8	0.1426	0.9760	28.94
5	12/19/77	0000	606	0.928	284.0	75.7	208.3	0.1393	0.9840	28.76
6	12/19/77	1600	607	0.925	284.4	75.7	208.7	0.1405	0.9889	29.05
<1-6>	-	-	-	-	-	-	-	-	0.9904 ± 0.0041	29.02 ± ~~0.1~~ 0.19

Mismatch will also increase the effective temperature of the cold load since some noise power radiated by the receiver out its input port will be reflected back into the receiver. The presence of an isolator in the receiver input waveguide assures that the noise power radiated out the receiver will be at nearly ambient temperature, and this was confirmed by observations of a shorting plate at the feed aperture. The effect of mismatch between the cold load and the receiver input (evaluated using (1) and adding the reflected signal) is to increase the effective radiation temperature of the cold load by about 1.6 K, while having essentially no effect on the ambient temperature load signal. Thus the cold load radiation temperature is approximately equal to $J(T_{LN}) + 1.9$ K = J(77.8 K) for typical conditions on Mt. Locke. The average value of the effective noise tube signal from Table V is 29.02 ± 0.19 K referred to the aperture of the main feed, where the error is estimated from the repeatability of the measurements. In addition to this random error, uncertainty in the load temperatures (conservatively estimated at ± 0.5 K each), in the foam wall loss (± 0.07 %), and in the mismatch correction (± 0.76 %) combine in quadrature to produce a total uncertainty in the thermal calibration scale of 1.06 %.

VI. ATMOSPHERIC EXTINCTION

The absorption of radio waves at 86.1 GHz by the terrestrial atmosphere is both significant and variable. Therefore accurate measurements of celestial sources must be accompanied by a nearly simultaneous determination of atmospheric opacity. In principle this can be done by

observing the decrease in received signal intensity as the effective air mass of the source increases. However, in this case atmospheric absorption cannot be separated from changing telescope gain (due to gravitational distortion). Furthermore, significant changes in atmospheric absorption can occur during the several hours usually required for such observations. Measurements of atmospheric emission, however, can be used to directly determine atmospheric absorption due to oxygen and water vapor. The two-layer model of Kutner [19] was used with ground temperature data to calculate the effective radiation temperatures of oxygen and water vapor. Surface absolute humidity measurements were also made to estimate the (variable) precipitable water vapor in a column and thus the relative absorption of water vapor [20] compared to the essentially constant oxygen component. From these values a weighted mean atmospheric radiation temperature was calculated and recorded for future use. The actual sky brightness temperature data were taken with the calibration horn rather than with the paraboloidal antenna, since the horn sidelobe levels were more accurately known than those of the paraboloid. Of course, the signal received by the horn is actually a convolution over 4π steradians of the horn power pattern and the brightness distribution of its surroundings. A computer model was constructed which included the effects of atmospheric emission, ground emission, cosmic microwave background emission, and reflection of horn backlobes by the paraboloid and by the receiver box. The apparent sky temperature $J(T_{SKY})$ is given by

$$J(T_{SKY}) = J(T_M)\ (1-e^{-\tau A}) + J(T_{BG})\ e^{-\tau A} \qquad (8)$$

where T_M is the calculated mean atmospheric radiation temperature {21} and T_{BG} is the microwave background brightness temperature (2.8 K) {22}. The zenith optical depth is τ, and the air mass A is given (to a good approximation for A<10) by

$$A = \frac{1}{\sin(E)} \qquad (9)$$

where E is the elevation angle. In this model the ground emission temperature is assumed to be the same as the surface ambient temperature. The measured radiation patterns of the calibration horn given in Fig. 2 were used for the computerized convolution, and the values of τ for each observing session were found by the method of least squares. The standard deviation of the differences between the computer model and the observed effective temperatures was typically only 0.3 K, indicating that the model quite accurately fits the shape of the sky tipping curve. Figure 7 shows the results of one such fit, and the values of zenith optical depth are given in Table VI. The values of τ are quite low (0.052-0.076) and are consistent with only 2-4 mm precipitable water vapor. The error in the atmospheric absorption correction to observed celestial source intensities was conservatively assumed to be 20% of the actual correction.

VII. DEPENDENCE OF REFLECTOR GAIN ON ELEVATION ANGLE

A series of observations were made on 24-27 November 1978 to determine if the peak gain of the paraboloid varies with elevation angle.

TABLE VI

ASTRONOMICAL DATA

Date	UTC (Hours)	Source	Number of Scans	$\tau \pm 1\sigma$ (Nepers)	Antenna	$T_A \pm 1\sigma$ (K)	$S \pm 1\sigma$ (Jy)	$T_B \pm 1\sigma$ (K)
12/17/77	2000	Sun	5	0.075 ± 0.015	Horn	229.9 ± 8.8	$(125.3 \pm 4.8) \times 10^6$	7985 ± 305
12/18/77	2000	Sun	11	0.053 ± 0.011	Horn	227.0 ± 5.6	$(123.8 \pm 3.0) \times 10^6$	7885 ± 193
12/18/77	0830	Jupiter	10	0.076 ± 0.015	Reflector	5.372 ± 0.102	1482 ± 28	175.3 ± 3.3
12/19/77	0730	Jupiter	10	0.052 ± 0.010	Reflector	5.542 ± 0.067	1529 ± 19	180.9 ± 2.2
12/19/77	1300	Saturn	4	0.052 ± 0.010	Reflector	0.747 ± 0.015	206 ± 4	153.4 ± 3.0
11/25,26, 27/78	1200	Jupiter	108	0.05 to 0.12	Reflector	4.205 ± 0.061	1160 ± 17	180.0 ± 2.6
11/24,25, 26,27/78	1700	Venus	56	0.05 to 0.12	Reflector	15.490 ± 0.420	4273 ± 116	357.5 ± 9.7

In order to accurately correct for rapid variations in atmospheric absorption, a rotating chopper wheel was used to produce a calibration signal according to the method first described by Davis and Vanden Bout {23} and later in detail by Ulich and Haas {24}. The resulting intensity scale is "corrected antenna temperature" (T_A^*), and is simply the antenna temperature that would be measured outside the terrestrial atmosphere with a lossless antenna. For a source which completely fills the forward beam, the corrected antenna temperature equals the source brightness temperature. Since the Sun is much larger in angular extent than either the main beam or the near sidelobes of the paraboloid power pattern, gravitational (or thermal) distortion of the reflector cannot affect the received signal by a significant amount. Thus observations of the Sun were used to check the accuracy of the atmospheric absorption corrections with the chopper-wheel calibration technique. As shown in Fig. 8, there is no indication of any change in measured solar intensity with elevation angle. The solar brightness temperature at 86.1 GHz measured with the 4.9 m paraboloid and the chopper-wheel calibration scheme is 7750 ± 150 K using a calculated beam coupling efficiency of 0.77; the error is due solely to receiver noise and atmospheric absorption corrections. Taking into account the uncertainty in telescope losses, the solar brightness temperature is 7750 ± 350 K. Concurrent observations of the planets Venus and Jupiter do show a slight increase in intensity from the horizon to the zenith, as shown in Fig. 9. The ratio of Venus to Jupiter was precisely measured when they were at equal elevation angles, and this ratio was used to place the Venus and Jupiter intensities on a common scale. Formally, a least squares fit of the relative antenna gain function of the

(assumed) form

$$G/G_o = 1 + \Delta G \sin (E) \qquad (10)$$

to the Sun data in Fig. 8 resulted in $\Delta G = 0.000 \pm 0.011$. For the planetary data in Fig. 9, $\Delta G = 0.020 \pm 0.015$, which indicates a slightly significant (2.0 ± 1.5 %) increase in gain at the zenith compared to the horizon, where the pattern range measurements were used to determine the absolute telescope gain.

Two other methods were used to check for gain variations with elevation angle. The first method was to compare the antenna half power beamwidths as measured on the pattern range with those inferred from Jupiter data at about 75^o elevation angle. Both E- and H-plane beamwidths were narrower (after correcting for the slight broadening due to the finite disk size of Jupiter) at 75^o elevation angle than at the horizon, inferring that $\Delta G = 0.018 \pm 0.018$. To derive this result, we have assumed that gravitational distortions are comparable in correlation length to the diameter of the paraboloidal reflector and thus that the power received by the main lobe remains constant. The second method was to determine the variation in the signal from Jupiter observed on 18 December 1977 after correction for atmospheric absorption utilizing the zenith optical depth obtained from the sky tipping procedure with the conical horn. This method gave $\Delta G = 0.027 \pm 0.023$. Thus all three methods of analysis are compatible with a total relative gain variation $\Delta G = 0.021 \pm 0.010$, and this weighted average was actually used to refer planetary intensities measured at positive elevation angles to the horizon, where the absolute gain calibration was previously accomplished.

VIII. ASTRONOMICAL OBSERVATIONS

A blackbody disk source of temperature T_B(K) which is small in angular size compared to the receiving antenna beamwidth will produce a measured incremental flux density S_M (W m^{-2} Hz^{-1}) at the surface of the Earth given by [24]

$$S_M = \frac{2k\nu^2\Omega_S C_S e^{-\tau A}}{c^2} \{ J(T_B)-J(T_{BG}) \} \qquad (11)$$

where c is the velocity of electromagnetic wave propagation in a vacuum (2.99793 x 10^8 m s^{-1}), Ω_S (sr), is the solid angle of the disk source, C_S is a normalized size correction factor to account for partial resolution of the disk by the antenna beam, and the other parameters have been previously defined. The solid angle correction factor C_S is given to a good approximation (when X < 0.4) by [24]

$$C_S = \frac{1 - e^{-X^2}}{X^2} \quad , \qquad (12)$$

where $X \equiv (4 \ln 2)^{\frac{1}{2}} R/\theta_A$ (13)

and R (rad) is the geometrical mean of the polar and equatorial semi-diameters of the (slightly elliptical) disk source and θ_A (rad) is the antenna half power beamwidth. The solid angle of the source is given by

$$\Omega_S = 2\pi \{ 1-\cos(R) \} \approx \pi R^2. \qquad (14)$$

The source flux density S that would be measured with no atmospheric loss is given by [24]

$$S \equiv S_M e^{\tau A} \equiv \frac{2k T_A}{\eta_A A_G} \qquad (15)$$

where T_A is the source antenna temperature (K), η_A is the antenna aperture efficiency, and A_G is the antenna geometrical collecting area (m^2). For cosmic radio sources the usual unit of flux density measurements is the Jansky ($1\ J_y \equiv 10^{-26}\ W\ m^{-2}\ Hz^{-1}$).

Observations of the Sun with the conical horn were made on two days in December 1977, and observations of Venus, Jupiter and Saturn were made with the paraboloidal reflector on 6 days in December 1977 and in November 1978. The peak source intensities were measured relative to the noise tube signal which was absolutely calibrated against the hot and cold loads. All measurements were corrected for pointing error by fitting a two dimensional gaussian function to the measured five point grid map to determine the peak intensity that would have beem measured with no pointing error. Saturn was observed alternately with the on-axis and the off-axis paraboloidal feeds to improve the signal-to-noise ratio. Separate measurements of Jupiter in each beam indicated a relative gain of the reference beam of 0.922 ± 0.010 times the gain of the main beam, and this value was used to normalize the Saturn observations. Calculations predict a gain reduction of about -0.4 dB for a feed 2.6 beamwidths off-axis [25], in agreement with the measurement. Table VI lists the antenna temperature, the flux density, and the brightness temperature for each data set. The quoted errors are the quadrature sums of the (1σ) random errors only and do not include the correlated systematic errors in antenna

gain or in thermal calibration. The angular source semidiameters were calculated for the time of each observation by dividing the known unit semidiameters {26} by the source distance in astronomical units. The Saturn brightness temperature has been calculated assuming that the rings do not emit or scatter radiation from the planet. Thus only the disk solid angle has been used in (14), although it has been corrected for polar tilt as seen from the Earth. At the time of these observations, the Saturnicentric latitude of the Earth (B) was -9.9^{o}, and the calculated disk solid angle has been corrected slightly to allow for this viewing angle.

IX. A NEW FLUX DENSITY SCALE

The average solar and planetary brightness temperatures and their total (random plus systematic) errors listed in Table VII may be used with (11) to establish an absolute flux density calibration scale near 86.1 GHz. This should be particularly useful for calibrating other millimeter wavelength antennas for radio astronomy purposes. An accurate and internally consistent intensity scale is needed for proper theoretical interpretation of astronomical observations, and the purpose of this experiment was to make such a scale routinely available to all millimeter wavelength observatories. The accuracy of the new 3.5 mm calibration scale may be judged by comparing these measurements with previously reported observations at nearby frequencies and with theoretical models. The 86.1 GHz solar brightness temperature measured with the conical horn is 7914 ± 192 K, which agrees with the value of 7750 ± 350 K determined by the chopper-wheel calibration technique using the 4.9 m reflector. Linsky {27} predicts

TABLE VII

86.1 GHZ DISK BRICHTNESS TEMPERATURES

Source	Disk Brightness Temperature (K)		Total 1σ Error (K)
Sun	7914	±	192
Venus	357.5	±	13.1
Jupiter	179.4	±	4.7
Saturn (B = -9.9^{o})	153.4	±	4.8

a brightness temperature of about 7800 ± 300 K at 86.1 GHz from his linear fit to a recalibrated solar spectrum. Thus the present measurements are in good agreement with previous observations. It should be noted that the solar brightness temperature determined by the horn measurements is an average over the unresolved visible disk, and any limb brightening will tend to increase the disk average temperature over the central brightness temperature which is sampled by high resolution antennas.

The 86.1 GHz brightness temperature of Saturn at $B = -9.9^{o}$ referred to the atmospheric disk only is 153.4 K with a random error of 3.0 K and a total error of 4.8 K. This result is in good agreement with both previous measurements {4}, {28} and with the theoretical spectrum of atmospheric emission {28}. However, the changing tilt angle of the rings as seen from the Earth introduces a slowly-varying component to Saturn's total 3 mm emission which may be as large as 15 K {28}. Thus Saturn is not a good calibration source for long time-base experiments at a few millimeters wavelength.

Jupiter's thermal brightness temperature is not known to be time-variable, and its constancy and large flux density make it the primary calibration source at millimeter wavelengths. Our observations indicate a brightness temperature for Jupiter of 179.4 K at 86.1 GHz, with a random error of 1.5 K and a total error of 4.7 K. A comparison with both the previously observed microwave spectrum {4}, {29} and with a convective model atmosphere {29} again shows agreement within the quoted errors.

At 86.1 GHz the measured brightness temperature of Venus is 357.5 K with a random error of 9.7 K and a total error of 13.1 K. At the time of these observations the planetocentric phase angle between the Sun and the Earth was $\underline{i} = 215^{o}$. Previous observations of Venus at 97.1 GHz {4} and at 88 GHz {30} are in agreement with this more precise result. At 88 GHz the reported mean temperature of Venus must be scaled upward by the ratio of the observed solar brightness temperature (7914 ± 192 K) to the assumed solar brightness temperature (6600 K), resulting in a Venus temperature of about 355 ± 32 K. Janssen {31} has calculated the millimeter-wavelength spectrum of Venus based on a model atmosphere which is consistent with all spacecraft and ground-based microwave observations. At 86.1 GHz the predicted disk brightness temperature is 363 ± 10 K, which also agrees with the observed temperature of 357.5 ± 13.1 K.

The measurements listed in Table VII define an absolute flux density scale which may be used to calibrate 3 mm radio astronomical observations to an accuracy (1σ) of about 3 %. The measured solar and planetary brightness temperatures are shown to agree with previous measurements at nearby wavelengths and with theoretical spectra.

ACKNOWLEDGMENT

The authors wish to thank A. J. Walker for assembling the receiver, R. B. Loren and W. L. Peters for programming assistance, and M. Thomas for typing the manuscript.

REFERENCES

{1} A. W. Straiton, "The absorption and reradiation of radio waves by oxygen and water vapor in the atmosphere," IEEE Trans. Antennas Propagat., vol. AP-23, pp. 595-597, 1975.

{2} A. J. Freiley, P. D. Batelaan, and D. A. Bathker, "Absolute flux density calibrations of radio sources: 2.3 GHz," NASA Tech. Memo. 33-806, Jet Propulsion Laboratory, 1977.

{3} G. T. Wrixon, W. J. Welch, and D. D. Thornton, "The spectrum of Jupiter at millimeter wavelengths," Astrophys. J., vol. 169, pp. 171-183, 1971.

{4} B. L. Ulich, J. R. Cogdell, and J. H. Davis, "Planetary brightness temperature measurements at 8.6 mm and 3.1 mm wavelengths," Icarus, vol. 19, pp. 59-82, 1973.

{5} B. L. Ulich, "Absolute brightness temperature measurements at 2.1-mm wavelength," Icarus, vol. 21, pp. 254-261, 1974.

{6} C. W. Tolbert, A. W. Straiton, and L. C. Krause, "A 16-foot millimeter wavelength antenna system, its characteristics and its applications," IEEE Trans. Antennas Propagat., vol. AP-13, pp. 225-229, 1965.

{ 7} J. R. Cogdell, J. J. McCue, P. D. Kalachev, A. E. Salomonovich, I. G. Moiseev, J. M. Stacey, E. E. Epstein, E. E. Altshuler, G. Feix, J. W. Day, H. Hvatum, W. J. Welch, and F. T. Barath, "High resolution millimeter reflector antennas," IEEE Trans. Antennas Propagat., vol. AP-18, pp. 515-529, 1970.

{ 8} B. L. Ulich, "A radiometric antenna gain calibration method," IEEE Trans. Antennas Propagat., vol. AP-25, pp. 218-223, 1977.

{ 9} V. D. Krotikov, V. A. Porfirjev, and V. S. Troitsky, "The development of the method of precise field intensity measurement and standardization of lunar radio emission at $\lambda = 3.2$ cm," Izvestia V.U.Z. Radiofizika, vol. 4, pp. 1004-1012, 1961.

{10} D. Russell and W. Larson, "RF attenuation," Proc. IEEE, vol. 55, pp. 942-959, 1967.

{11} W. N. Hardy, "Precision temperature reference for microwave radiometry," IEEE Trans. Microwave Theory Tech., vol. MTT-21, pp. 149-150, 1973.

{12} C. A. Balanis, "Dielectric constant and loss tangent measurements at 60 and 90 GHz using the Fabry-Perot interferometer," Microwave J., vol. 14, no. 3, pp. 41-44, 1971.

{13} A. F. Kay, "Radomes and absorbers," in Antenna Engineering Handbook, H. Jasik, Ed. New York: McGraw Hill, 1961, p. 32-30.

{14} S. Silver, Ed., Microwave Antenna Theory and Design. Lexington, MA: Boston Tech., 1964, pp. 439-443.

{15} N. Kuhn, "How accurate is your power meter?," Microwaves, vol. 16, no. 9, pp. 106-114, 1977.

{16} R. C. Johnson, H. A. Ecker, and J. S. Hollis, "Determination of far-field antenna patterns from near-field measurements," Proc. IEEE, vol. 61, pp. 1668-1694, 1973.

{17} J. J. Stangel and W. M. Yarnall, "Pattern characteristics of an antenna focused in the Fresnel region," IRE Int. Conv. Record, part 1, pp. 3-12, March 26-29, 1962.

{18} C. T. Stelzried, "Microwave thermal noise standards," IEEE Trans. Microwave Theory Tech., vol. MTT-16, pp. 646-655, 1968.

{19} M. L. Kutner, "Application of a two-layer atmospheric model to the calibration of millimeter observations," Astrophys. Lett., vol. 19, pp. 81-87, 1978.

{20} F. I. Shimabukuro and E. E. Epstein, "Attenuation and emission of the atmosphere at 3.3 mm," IEEE Trans. Antennas Propagat., vol. AP-18, pp. 485-490, 1970.

{21} V. J. Falcone, K. N. Wulfsberg, and S. Gitelson, "Atmospheric emission and absorption at millimeter wavelengths," Radio Science, vol. 6, pp. 347-355, 1971.

{22} A. A. Penzias, "Cosmology and microwave astronomy," in Cosmology, Fusion, and Other Matters, F. Reines, Ed. Boulder, CO: Colorado Associated University, 1972, pp. 29-47.

{23} J. H. Davis and P. Vanden Bout, "Intensity calibration of the interstellar carbon monoxide line at λ 2.6 mm," Astrophys. Lett., vol. 15, pp. 43-47, 1973.

{24} B. L. Ulich and R. W. Haas, "Absolute calibration of millimeter-wavelength spectral lines," Astrophys. J. (Supplement Series), vol. 30, pp. 247-258, 1976.

{25} J. W. Baars, "Characteristics of the paraboloidal reflector antenna," Electronics Division Internal Report No. 57, National Radio Astronomy Observatory, 1966.

{26} The American Ephemeris and Nautical Almanac for the Year 1979. Washington, D. C.: U. S. Gov. Printing Office, 1977, pp. 541, 546.

{27} J. L. Linsky, "A recalibration of the quiet Sun millimeter spectrum based on the Moon as an absolute radiometric standard," Solar Physics, vol. 28, pp. 409-418, 1973.

{28} M. J. Klein, M. A. Janssen, S. Gulkis, and E. T. Olsen, "Saturn's microwave spectrum: implications for the atmosphere and the rings," in The Saturn System, D. M. Hunten and D. Morrison, Eds. Springfield, VA: National Technical Information Service, 1978, pp. 195-216.

{29} G. L. Berge and S. Gulkis, "Earth-based radio observations of Jupiter: millimeter to meter wavelengths," in Jupiter, T. Gehrels, Ed. Tucson, AZ: University of Arizona, 1976, pp. 621-692.

{30} E. E. Epstein, J. P. Oliver, S. L. Soter, R. A. Schorn, and W. J. Wilson, "Venus: on an inverse variation with phase in the 3.4-mm emission during 1965 through 1967," Astron. J., vol. 73, pp. 271-274, 1968.

{31} M. Janssen, private communication, 1979.

FIGURE CAPTIONS

Fig. 1. Measured radiation patterns of 4.9 m paraboloidal antenna at 86.1 GHz. The asymmetry of the first sidelobes indicates the presence of coma due to a slight lateral offset of the feed horn from the axis of the paraboloid. (a) In hour angle (H-plane). (b) In declination (E-plane).

Fig. 2. Measured radiation patterns of conical horn at 86.1 GHz. (a) In hour angle (H-plane). (b) In declination (E-plane).

Fig. 3. Spillover efficiency of conical horn at 86.1 GHz calculated from measured patterns in Fig. 2.

Fig. 4. Block diagram of transmitter with feedback circuits to stabilize frequency and output power.

Fig. 5. Block diagram of receiver with narrowband and wideband IF systems and integral reflectometer.

Fig. 6. Variation in transmitter power received by the 4.9 m antenna over a 12.9 km pattern range (1235 UTC on 15 December 1977).

Fig. 7. Measured effective antenna temperature of the calibration horn as a function of air mass (1530 UTC on 19 December 1977). The solid line is the computer convolution model fit to the observations with a zenith optical depth of 0.052 Np. With no atmosphere present (air mass = 0), the effective antenna temperature of the 2.8 K cosmic background radiation is about 1.2 K at 86.1 GHz.

Fig. 8. Measured corrected antenna temperatures of the Sun at 86.1 GHz with the 4.9 m paraboloid as a function of elevation angle. The solid line is the result of the least squares fit of the variable gain model described in the text with $\Delta G = 0.000 \pm 0.011$.

Fig. 9. Measured planetary corrected antenna temperatures at 86.1 GHz with the 4.9 m paraboloid as a function of elevation angle. The solid line is the result of the least squares fit of the variable gain model described in the text with $\Delta G = 0.020 \pm 0.015$.

Fig. 1a

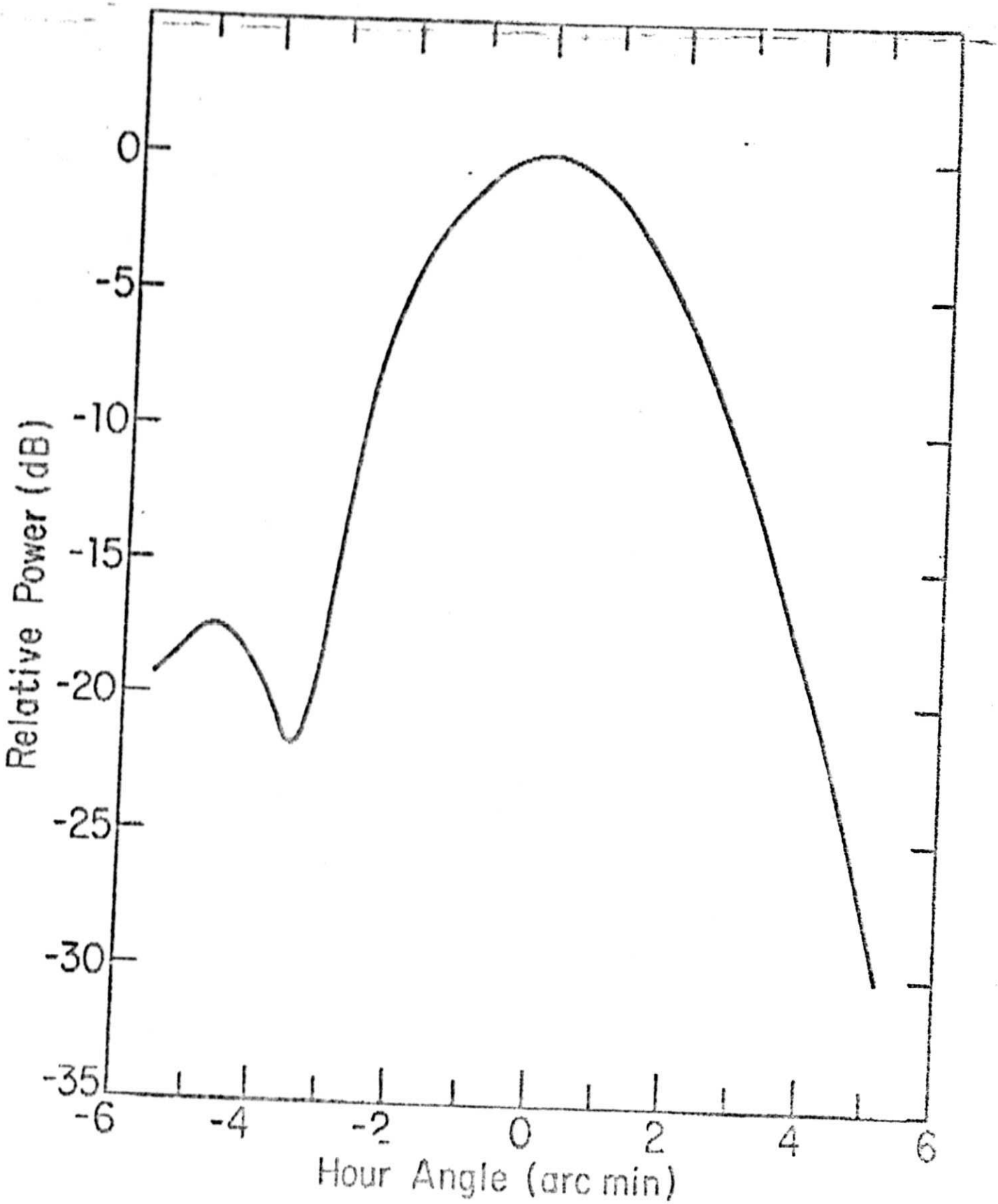
0
-5
-10
-15
-20
-25
-30
-35
Relative Power (dB)
-6
-4
-2
0
2
4
6
Hour Angle (arc min)

Fig. 16

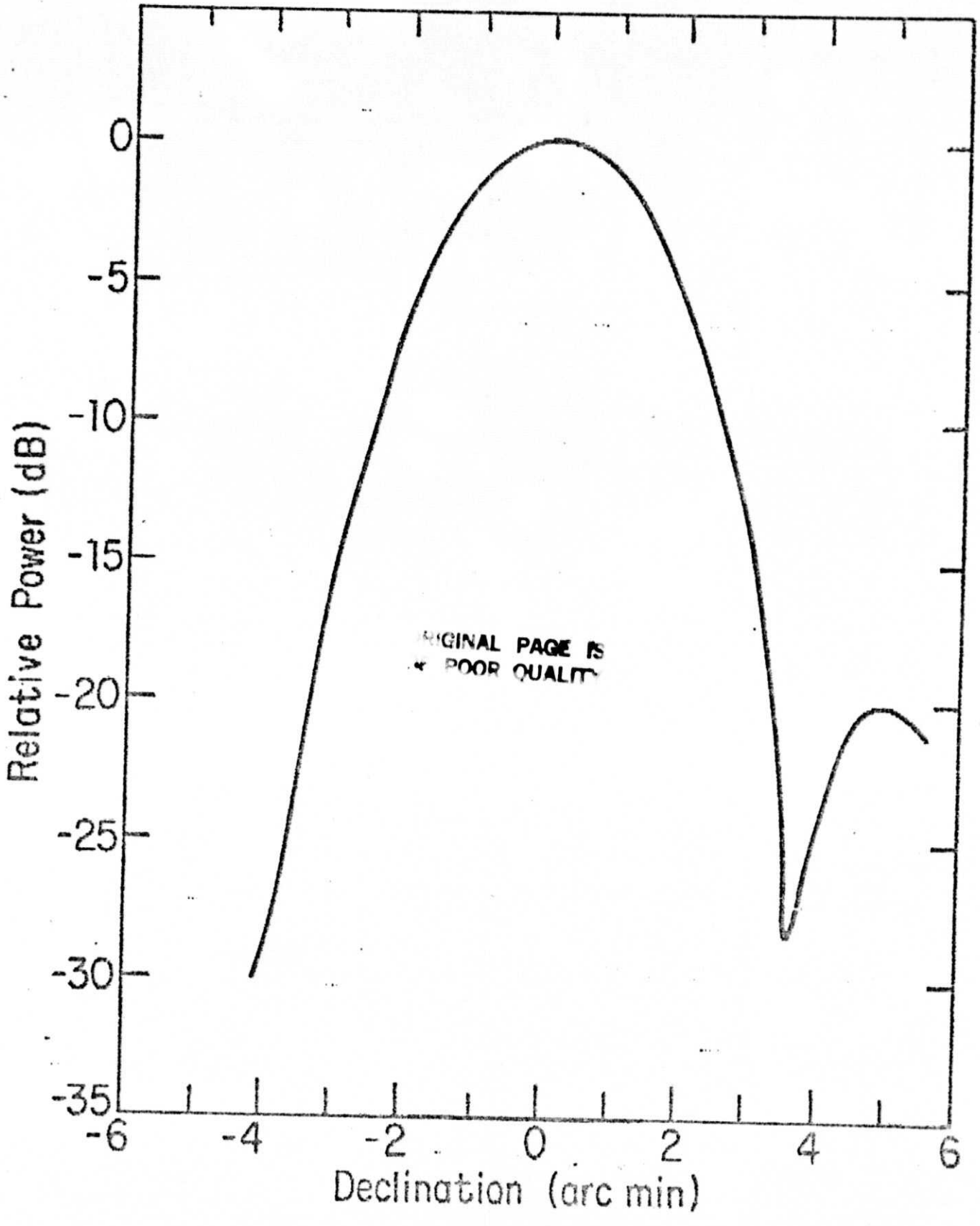

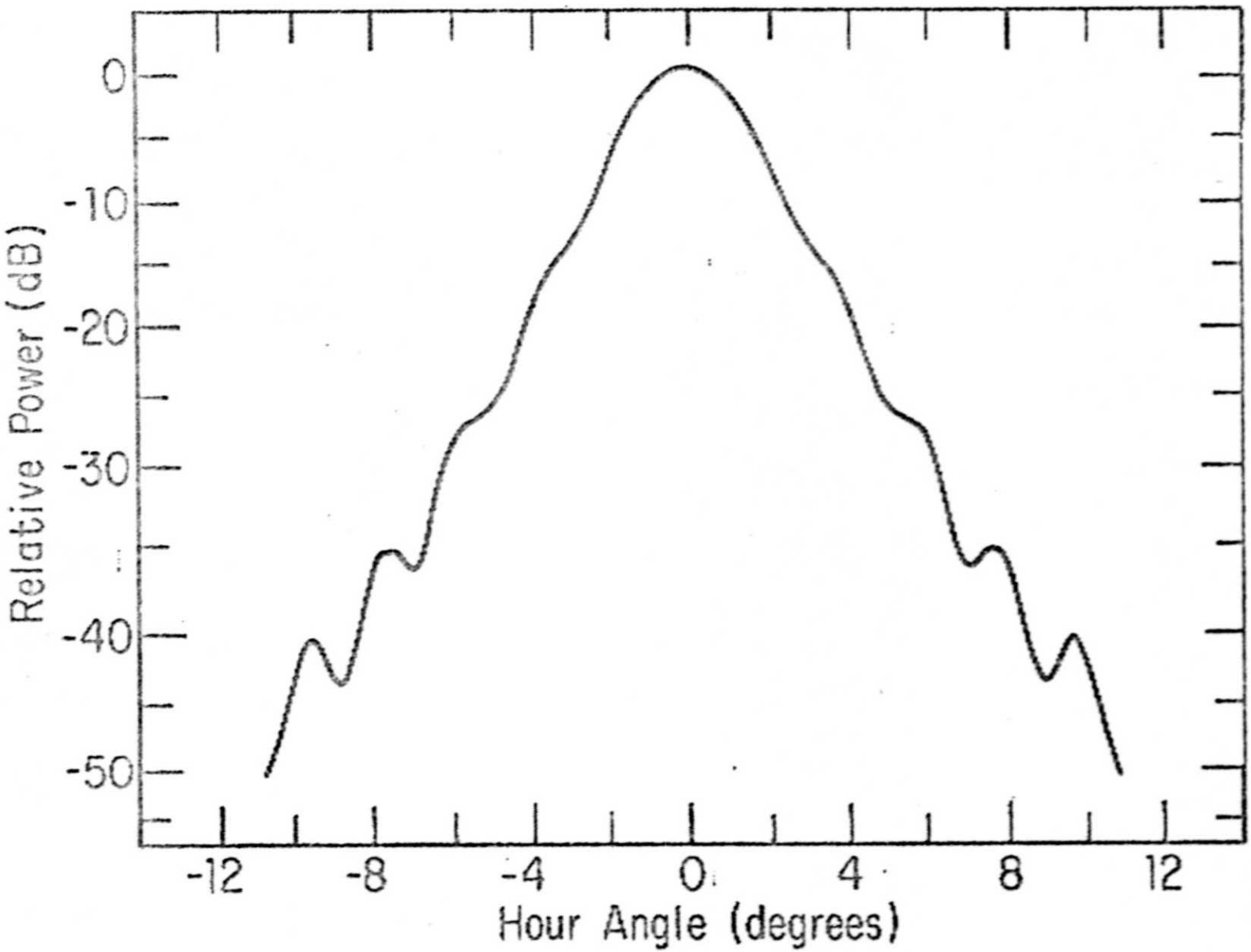
0
-10
-20
-30
-40
-50
Relative Power (dB)
-12
-8
-4
0
4
8
12
Hour Angle (degrees)

Fig. 2a

Fig. 2b

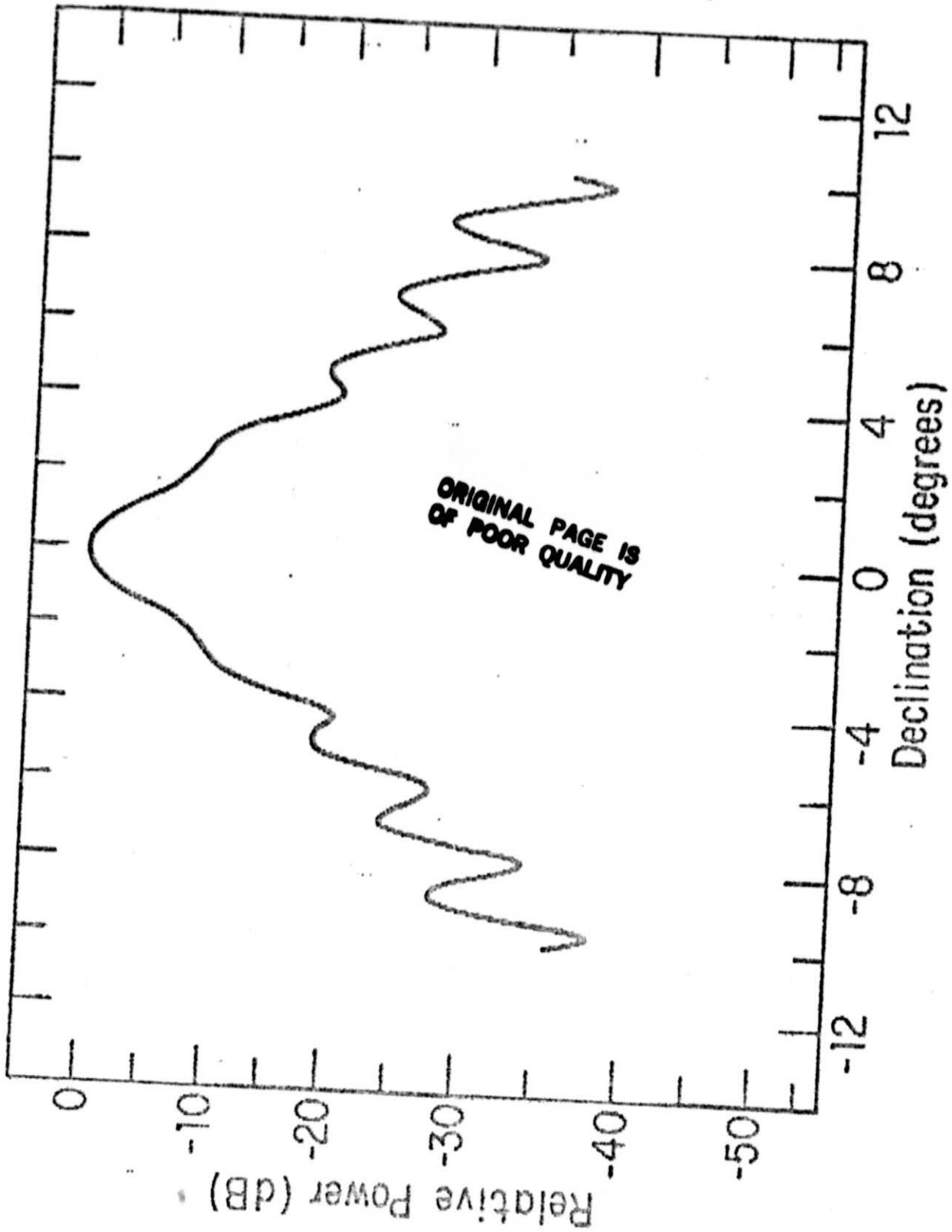
Relative Power (dB)
0
-10
-20
-30
-40
-50
-12
-8
-4
0
4
8
12
Declination (degrees)
ORIGINAL PAGE IS
OF POOR QUALITY

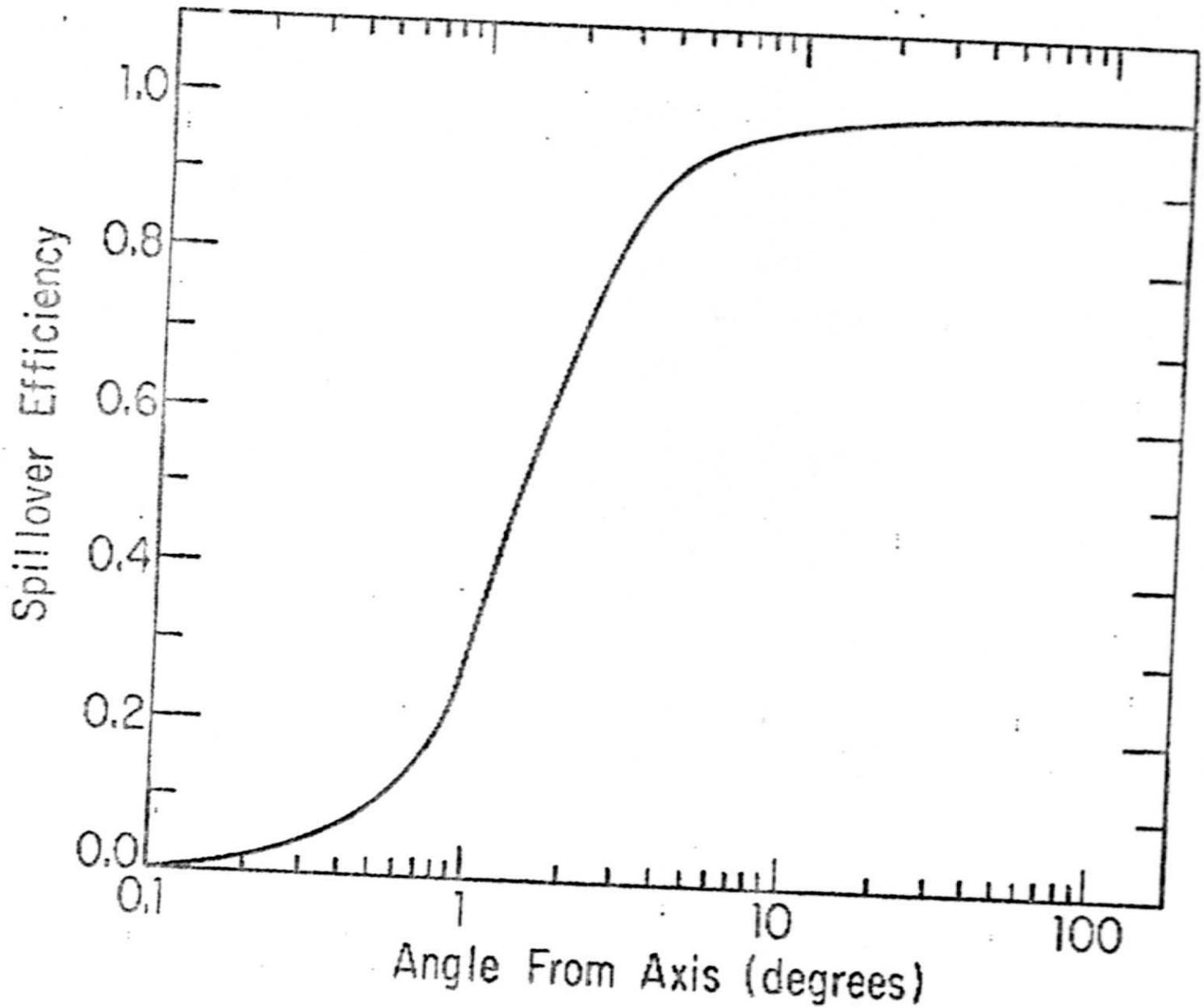
Spillover Efficiency
1.0
0.8
0.6
0.4
0.2
0.0
0.1
1
10
100
Angle From Axis (degrees)

Fig. 3

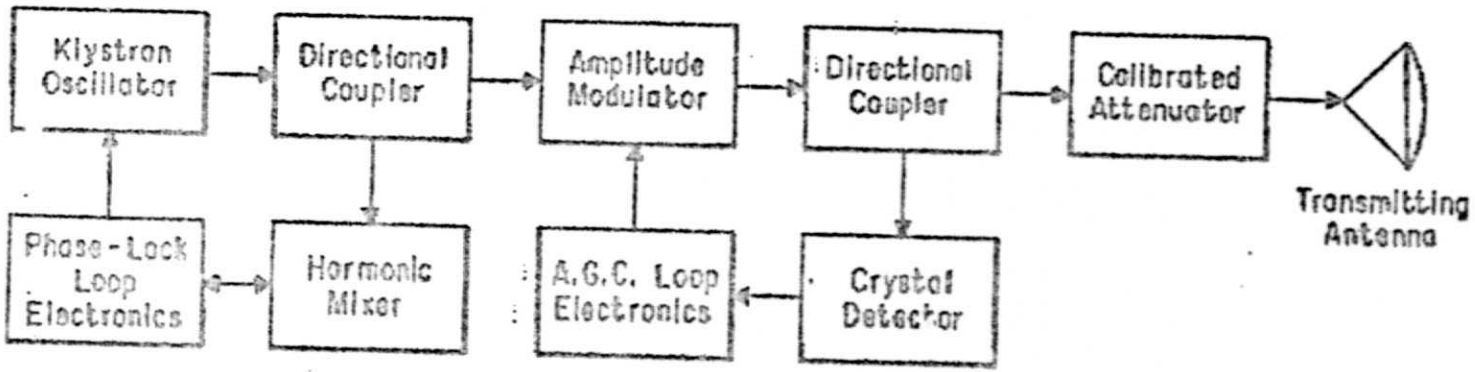

Fig. 4

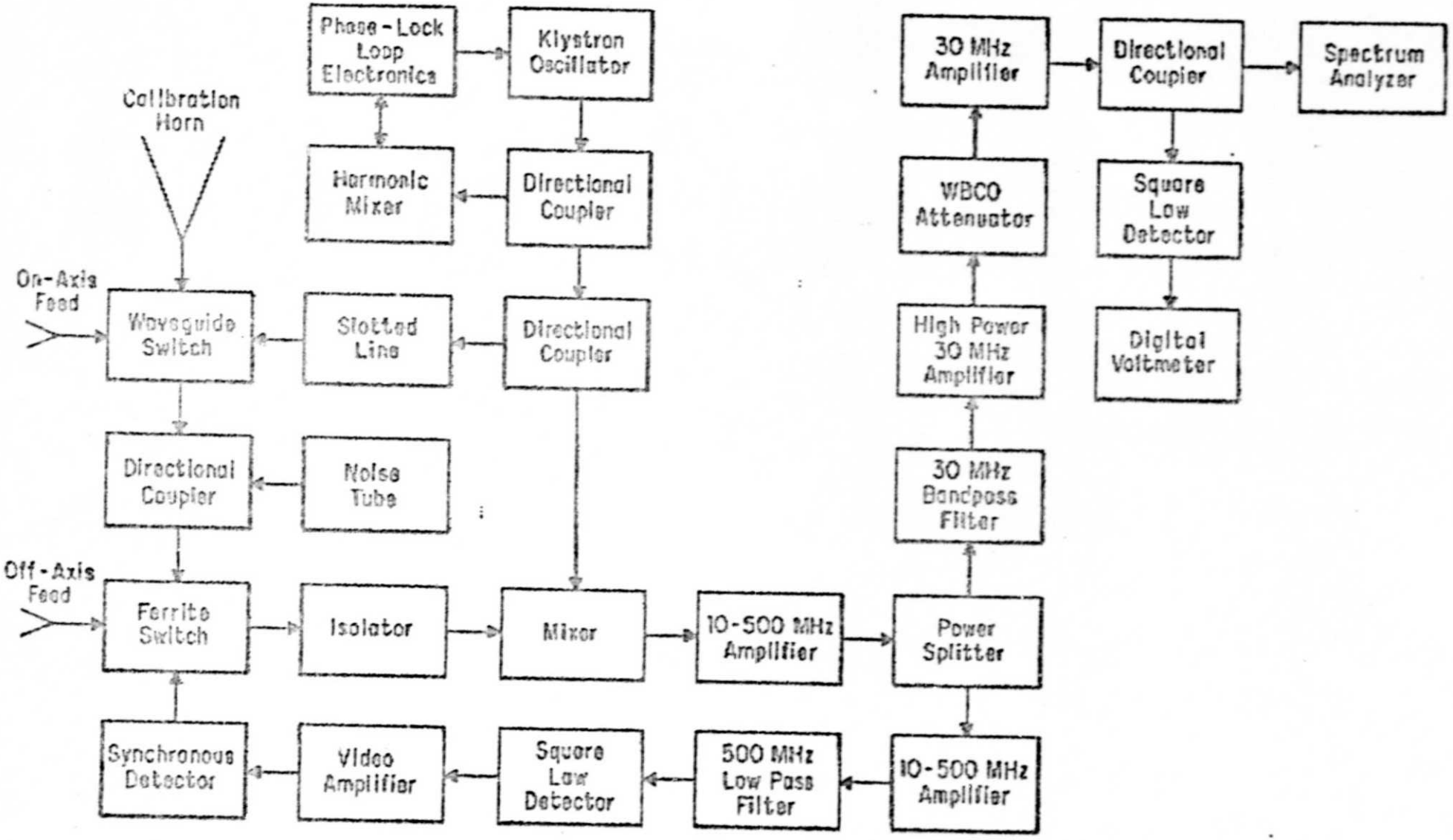
Phase-Lock Loop Electronics
Klystron Oscillator
30 MHz Amplifier
Directional Coupler
Spectrum Analyzer
Calibration Horn
Harmonic Mixer
Directional Coupler
WBCO Attenuator
Square Law Detector
On-Axis Feed
Waveguide Switch
Slotted Line
Directional Coupler
High Power 30 MHz Amplifier
Digital Voltmeter
Directional Coupler
Noise Tube
30 MHz Bandpass Filter
Off-Axis Feed
Ferrite Switch
Isolator
Mixer
10-500 MHz Amplifier
Power Splitter
Synchronous Detector
Video Amplifier
Square Law Detector
500 MHz Low Pass Filter
10-500 MHz Amplifier

Fig. 5

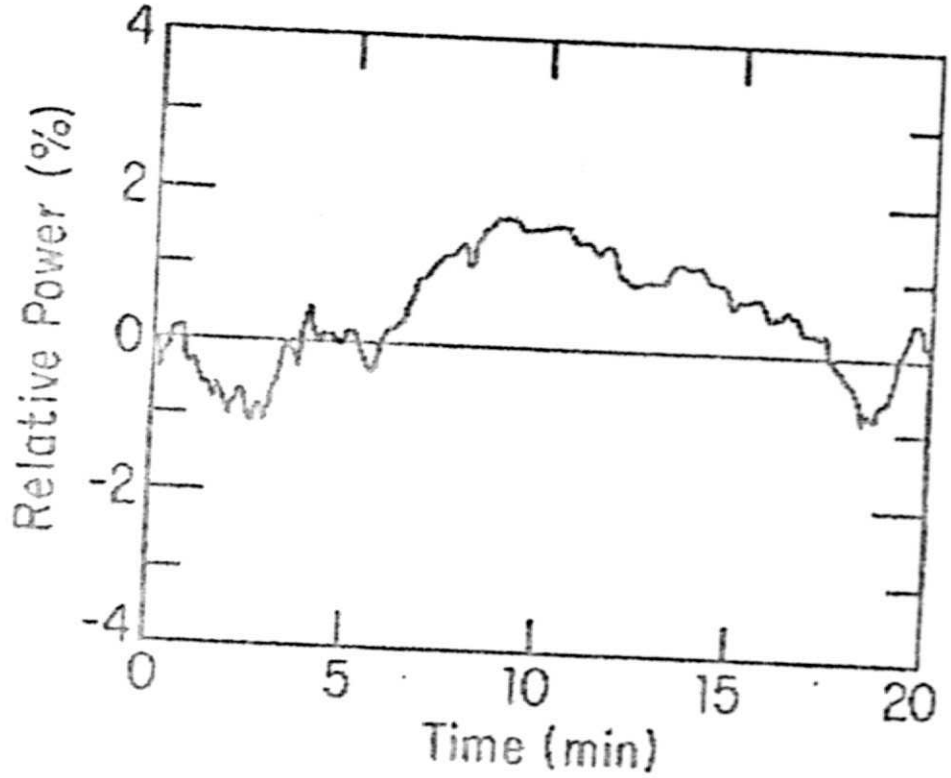

Fig. 6

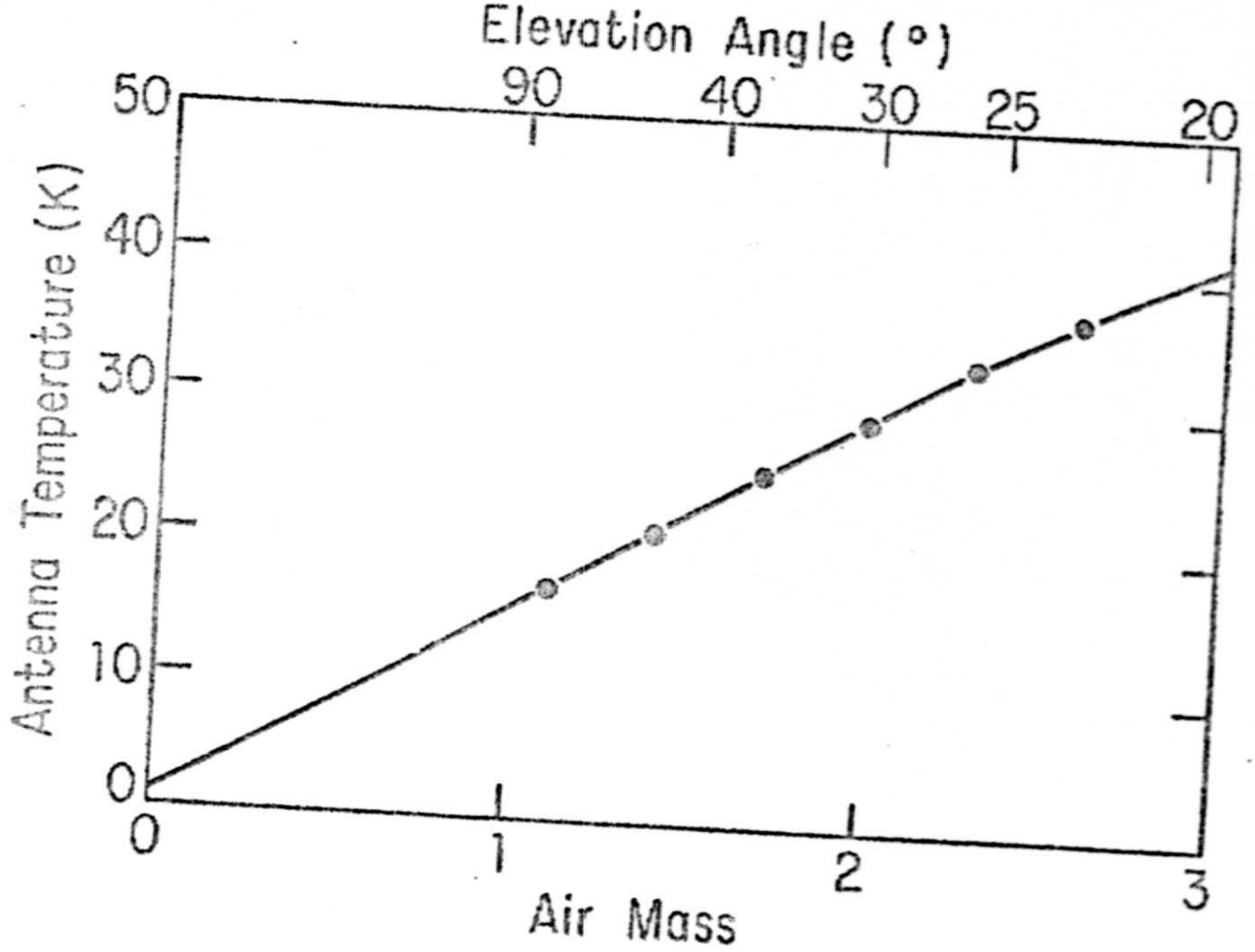
Elevation Angle (°)
90
40
30
25
20
Antenna Temperature (K)
50
40
30
20
10
0
0
1
2
3
Air Mass

Fig. 7

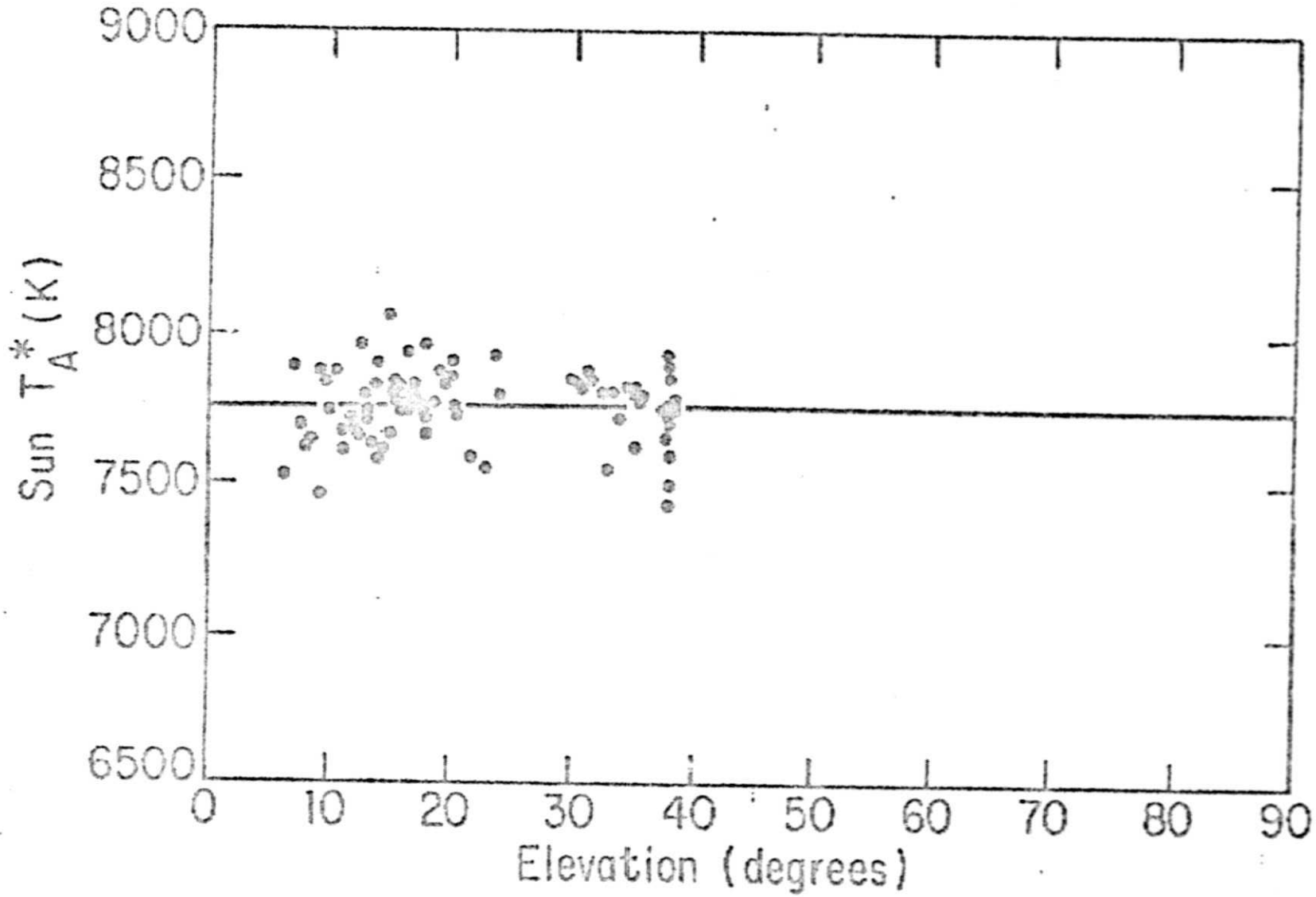
9000
8500
8000
7500
7000
6500
Sun T_A^* (K)
0
10
20
30
40
50
60
70
80
90
Elevation (degrees)

Fig. 8

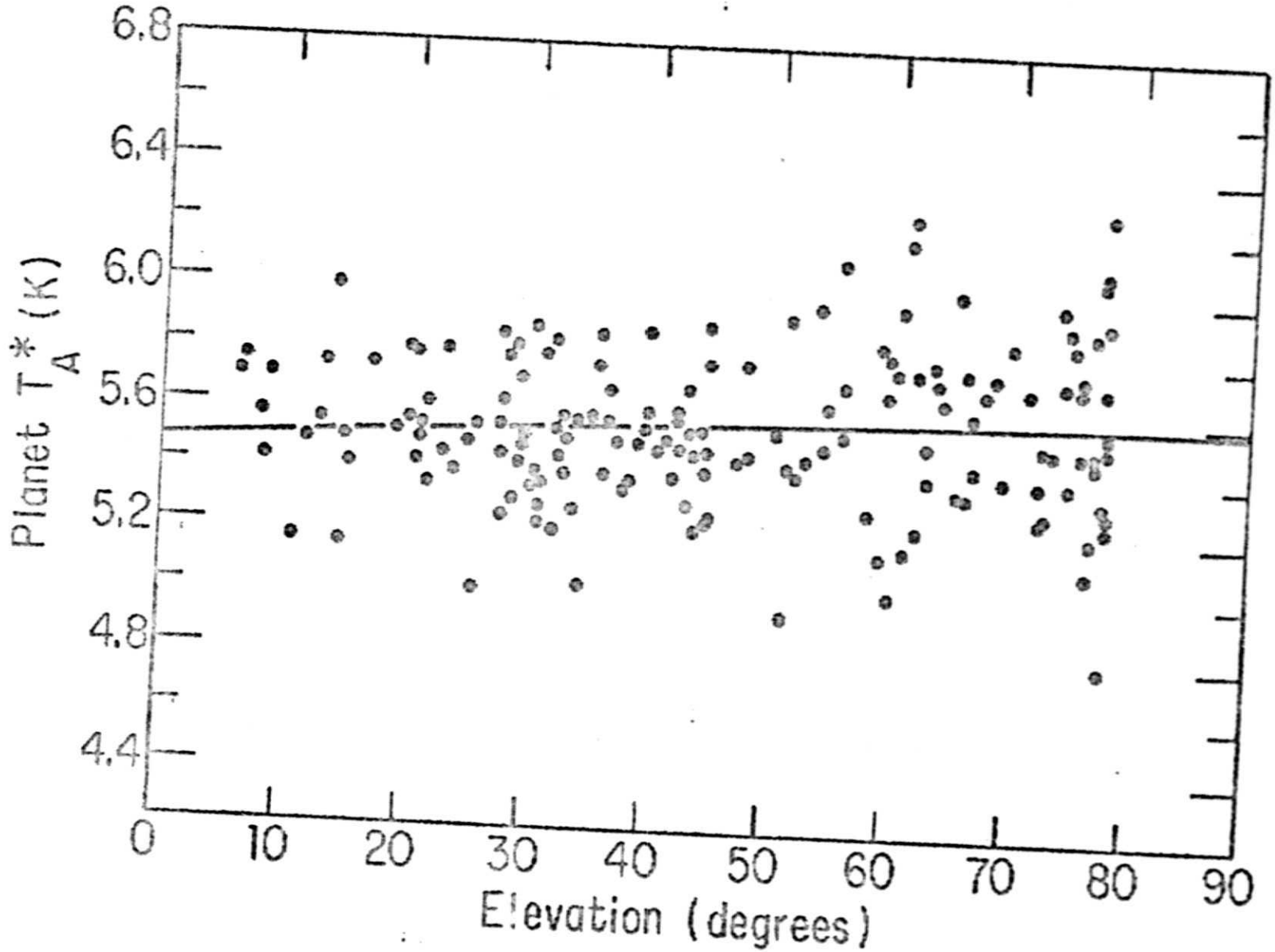
6.8
6.4
6.0
5.6
5.2
4.8
4.4
Planet T_A^* (K)
0
10
20
30
40
50
60
70
80
90
Elevation (degrees)

Fig. 9